ELSEVIER

Journal of Photochemistry and Photobiology A: Chemistry 120 (1999) 63–74

Journal of Photochemistry and Photobiology A:Chemistry

Photocatalyzed degradation of polymers in aqueous semiconductor suspensions. IV Theoretical and experimental examination of the photooxidative mineralization of constituent bases in nucleic acids at titania/water interfaces

Satoshi Horikoshi[a], Nick Serpone[b], Shuji Yoshizawa[a], John Knowland[c], Hisao Hidaka[a,*]

[a]*Frontier Research Center for the Global Environment Protection and Department of Chemistry, Meisei University, 2-1-1 Hodokubo, Hino, Tokyo 191-8506, Japan*

[b]*Department of Chemistry and Biochemistry, Concordia University, 1455 de Maisonneuve Blvd. West, Montreal, Que., Canada H3G 1M8*

[c]*University of Oxford, Department of Biochemistry, South Parks Road, Oxford OX1 3QU, UK*

Received 14 May 1998; received in revised form 13 August 1998; accepted 21 September 1998

Abstract

The mechanistic sequence(s) in the TiO_2-photocatalytic oxidation of constituent pyrimidine and purine bases in nucleic acids is examined theoretically by molecular orbital calculations of frontier electron densities and point charges on all atoms, and experimentally by UV–Vis spectroscopy and gas chromatography to assess how the chemical structure of the bases affects their photocatalyzed mineralization. Rates of formation of NH_4^+ and NO_3^- ions in the pyrimidine bases are closely dependent on the existence of the carbonyl and amino groups; for example, formation of NO_3^- ions is faster than formation of NH_4^+ ions for uracil (Ura) and thymine (Thy) having the carbonyl function. By contrast, NH_4^+ ions are produced faster than NO_3^- ions in the case of cytosine (Cyt) which possesses a primary amine function. In comparison with uric acid, which has no amino group, the photocatalyzed mineralization of the purine bases adenine (Ade) and guanine (Gua) generates a greater quantity of NH_4^+ ions than NO_3^- ions, in the initial stages. In nearly all cases examined, formation of NO_3^- ions takes place only after an induction period and originates mostly from the ring nitrogen atoms of the bases.

Keywords: Photooxidation; Photodegradation; Pyrimidine base; Purine base; Molecular orbital calculations; Photocatalysis; Titanium dioxide

1. Introduction

The photodegradation of several classes of organic compounds catalyzed by TiO_2 semiconductor particulates, with a particular emphasis on the photocatalytic purification and treatment of water and air, has been described in numerous publications in the last few years [1]. Two of our laboratories have been actively engaged in extensive examination of the photocatalyzed oxidation and/or reduction of organic {surfactants [2–5], agrochemicals [6–8], polymers [9–12]} and inorganic {cyanide [13], organometallic compounds [14,15]} pollutants at the TiO_2/water interface. Sterilization of microorganisms such as bacteria, fungi, mold, and virus among others, has been successfully demonstrated in illuminated TiO_2 dispersions [16–23]. The elimination or growth suppression of cancer cells in vivo by illuminated TiO_2 particulates has also been achieved [24–27]. However, mechanistic steps at the molecular level have not yet been explored. Titania particles present in sunscreen lotions have been shown to pose a potential risk to skin when illuminated with UV-A and/or UV-B sunlight. Photodamage caused to DNA by TiO_2 sunscreen agents under simulated sunlight was reported recently [28].

Tentative processes have been inferred in the photocatalytic mineralization of amino acids [29] and nucleic acids [30]. However, the inferred mechanistic steps were rendered conjectural by the complexity of the various structures surveyed. The double helix of DNA is made possible by the hydrogen bonds joining the respective pyrimidine and purine bases. Details of the photomineralization pathways of these bases and the respective rates of formation of NH_4^+ and NO_3^- ions have not been reported.

*Corresponding author. E-mail: hidaka@chem.meisei-u.ac.jp

1010-6030/99/$ – see front matter
PII: S1010-6030(98)00408-0

In this study we explore the photomineralization of the constituent pyrimidine and purine bases in nucleic acids by UVA/UVB illuminated TiO_2 particulates in aqueous suspensions. Specifically, we report on the formation of NH_4^+ and NO_3^- ions and the corresponding kinetics, temporal changes or formation of the primary amine function, evolution of CO_2 and N_2 gases, temporal variations in the UV absorption spectra of the bases and simulation of the UV spectra by frontier electron density calculations. Mechanistic steps are discussed from the standpoint of the chemical structure of the various bases, the point charges and frontier electron densities, and of the modes of adsorption of the substrates on the TiO_2 particle surface. The position of $^{\bullet}OH$ radical attack was estimated by UV-spectral simulation and the experimental data as well as molecular orbital (MO) calculations in the photodecomposition of pyrimidine and purine bases. With the present survey we hope to establish a learning curve from which we might begin to understand the initiation of the photooxidative process at the photocatalyst/solution interface.

2. Experimental

2.1. Chemicals and reagents

Samples of the pyrimidine bases uracil (Ura: $C_4H_4N_2O_2$), thymine (Thy: $C_5H_6N_2O_2$) and cytosine (Cyt: $C_4H_5N_3O$), and of the purine bases adenine (Ade: $C_5H_5N_5$) and guanine (Gua: $C_5H_5N_5O$), and uric acid were supplied by Tokyo Kasei. The photocatalyst titanium dioxide was Degussa P-25 (particle size, 20–30 nm by TEM microscopy; 87% anatase and 13% rutile determined by X-ray diffraction; surface area, 53 $m^2\ g^{-1}$ by BET methods).

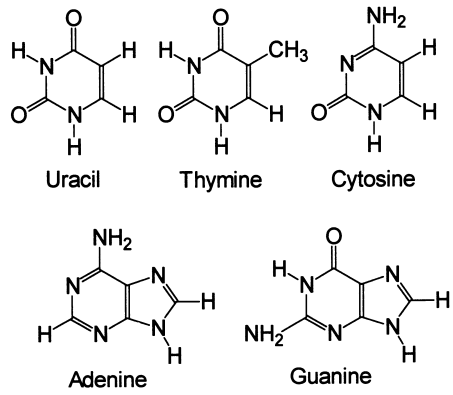

2.2. Photodegradation procedures and analytical methods

Ion-exchanged water (pH = 6.3) was used to make up solutions containing the pyrimidine or purine base (0.1 mM in 50 ml) and 50 mg of TiO_2 particulates placed in a 124-ml reactor. Irradiation of the dispersions was carried out with a 75-W mercury lamp, which delivered 2.46 mW cm^{-2} in the wavelength range 310–400 nm (maximum emission at $\lambda = 360$ nm).

The primary amine function was quantitatively determined by spectrofluorometric analysis by the following general procedure: the illuminated solution was sampled (0.15 ml) and mixed with 0.15 ml of borate buffer (pH = 9) to which was then added 0.15 ml of fluorescamine solution (0.03%) dissolved in acetone. The resulting solution was analyzed with a JASCO FP-770 spectrofluorometer. Opening of the base rings was analyzed with a JASCO UVIDEC 660 spectrophotometer. The concentration of ammonium and nitrate ions was assayed employing a JASCO liquid chromatograph (HPLC) equipped with a CD-5 conductivity detector and either a Y-521 cation column or an I-524 anion column. The temporal evolution of N_2 and CO_2 was monitored by gas chromatography with an Ookura Riken chromatograph (model 802; TCD detection) through either a Molecular sieve 5A (N_2 gas) or a Porapack Q (CO_2 gas) column with helium as the carrier gas. Each rate constant for CO_2 evolution, N_2 evolution and NH_4^+ and NO_3^- ions formation was calculated as a pseudo first order reaction. The temporal change of the ζ-potential on irradiation was measured with an Otsuka electrophoretic light scattering equipment.

2.3. Molecular orbital calculations

Molecular orbital (MO) calculations were carried out at the single determinant (Hartree-Fock) level with the optimal conformation having minimum energy obtained at the AM1 level. All semi-empirical calculations were performed with the MOPAC version 6 using the CAChe system implemented on a Power Macintosh computer. Where all MO calculations were simulated for the initial processes of $^{\bullet}OH$ radical attack and adsorption of base molecules on TiO_2 surface, but not for the formation of amounts of NH_4^+ and NO_3^- ions. The UV absorption spectra were simulated using the ZINDO version 6.3 also available in the CAChe system.

3. Results and discussion

TiO_2 particles absorb UV light of energy greater than the bandgap (ca. 3.2 eV) to generate electron/hole pairs (Eq. (1)). Following various steps, the holes (h^+) are ultimately trapped by HO^- ions or by H_2O at the particle surface to yield H^+ and $^{\bullet}OH$ radicals (Eq. (2)). Our data do not preclude the possibility of direct hole scavenging by the base to form cation radicals, however, under our conditions, this scenario is rather unlikely. Concomitantly, dioxygen molecules react with electrons (e^-) in the conduction band to yield superoxide radical anions, $O_2^{\bullet -}$, which on protonation generates the hydroperoxy, $^{\bullet}OOH$, radicals (Eqs. (3) and (4)).

$$TiO_2 + h\nu \overset{h\nu > E_{bg}}{\rightarrow} TiO_2(e_{cb}^- + h_{vb}^+) \rightarrow e_{cb}^- + h_{vb}^+ \quad (1)$$

$$h^+ + H_2O\ (\text{or } OH_{surf.}^-) \rightarrow {}^{\bullet}OH + H^+ \quad (2)$$

$$e_{cb}^- + O_2 \rightarrow O_2^{\bullet -} \quad (3)$$

$$O_2^{\bullet -} + H^+ \rightarrow {}^{\bullet}OOH \quad (4)$$

$$^{\bullet}OH\ (\text{or}\ ^{\bullet}OOH) + \text{base} \rightarrow\rightarrow \text{Oxidative products} \quad (5)$$

The electrical charge of the TiO_2 particle surface is positive due to an excess of protons from H_2O (Eq. (2)) or from the solution if acidic. Accordingly, the negatively charged atoms in the structure of the bases will be attracted on the surface of TiO_2 by simple coulombic forces, and thus $^{\bullet}OH$ radicals photogenerated on the TiO_2 surface are expected to be the major oxidative agents to attack the adsorbed substrates.

4. Photodegradation of pyrimidine bases

4.1. Uracil

The temporal generation of NH_4^+ and NO_3^- ions and the formation of a primary amine during illumination of the TiO_2/Ura dispersion are shown in Fig. 1(a). The rate of formation of NH_4^+ ions ($k \approx 0.5 \pm 0.2\ h^{-1}$) was greater than the rate of NO_3^- ion production ($k = 0.09 \pm 0.03\ h^{-1}$; see Table 1), reaching a maximal concentration of ca. 0.12 mM; no further evolution of ammonia occurred after 8 h of illumination but formation of NO_3^- ions continued. The concentration of the primary amine, determined by the emission intensity of the fluorescamine solution, decreased initially as ammonia evolved and subsequently increased to its maximal value after ca. 3 h of further UV exposure. Formation of NO_3^- ions exhibited a 6-h induction period, coinciding with a decrease in the concentration of the primary amine the origin of which might also be a point of origin for the formation of NO_3^- ions. Production of the primary amine proceeded up to 15 h of illumination in competition with added formation of NO_3^- ions after which it decreased as nitrate ion evolution continued.

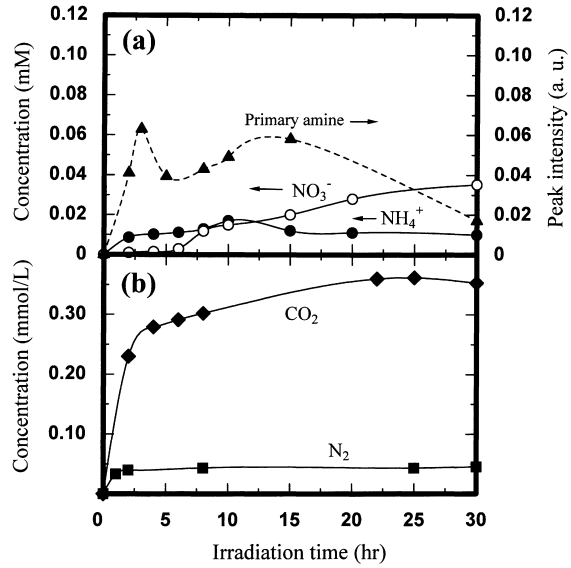

Fig. 1. Photodegradation of uracil (a): formation of NH_4^+ and NO_3^- ions, and generation of primary amine, (b): evolution of CO_2 and N_2 gas.

The temporal evolution of nitrogen gas ($k = 1.2 \pm 0.1\ h^{-1}$) and carbon dioxide gas produced via biphasic kinetics ($k_1 = 1.2 \pm 0.5\ h^{-1}$ and $k_2 = 0.11\ h^{-1}$) during the photooxidative degradation of Uracil is illustrated in Fig. 1(b). Approximately 47% of the total concentration of nitrogen atoms from uracil was converted to nitrogen gas after 30 h of illumination of the TiO_2/Ura suspension to give a global photomineralization yield for NH_4^+ ions, NO_3^- ions and N_2 gas of 70%. By comparison, about 0.35 mmol/l of carbon dioxide had evolved after this period, representing a mineralization yield of ca. 88% for all the carbon atoms in uracil; a large fraction of the yield (~ 0.30 mmol/l) was

Table 1
Kinetics of formation of NO_3^- and NH_4^+ ions and CO_2 and N_2 gases, and percent yields of conversion in the photooxidative mineralization of pyrimidine and purine base (0.1 mM) constituents in nucleic acids

	Uracil	Thymine	Cytosine	Adenine	Guanine
$k(NO_3^-)$, h^{-1}	0.09 ± 0.03[a]	0.08 ± 0.03[a]	0.16 ± 0.02	0.061 ± 0.008[b]	0.018 ± 0.006
$\{t_{1/2}$, h$\}$	(7.7)	(8.7)	(4.3)	(11.4)	(38)
$[NO_3^-]$, mM[c]	0.035	0.062	0.018	0.088	0.11
$k(NH_4^+)$, h^{-1}	0.5 ± 0.2	ca. 0.02	0.6 ± 0.2	0.35 ± 0.04	0.16 ± 0.02
$\{t_{1/2}$, h$\}$	(1.3)	(37)	(1.2)	(1.9)	(4.4)
$[NH_4^+]$, mM[c]	0.010	0.013	0.015	0.10	0.065
$k(CO_2)$, h^{-1}	1.2 ± 0.5	0.28 ± 0.03	0.32 ± 0.03	0.19 ± 0.03	0.23 ± 0.04
$\{t_{1/2}$, h$\}$	(0.6)	(2.5)	(2.2)	(3.6)	(3.0)
$[CO_2]$, mmol/l[c]	0.35	0.35	0.36	0.45	0.35
$k(N_2)$, h^{-1}	1.2 ± 0.1	0.16 ± 0.02	0.4 ± 0.2[b]	0.38 ± 0.05	0.15 ± 0.04
$\{t_{1/2}$, h$\}$	(0.6)	(4.4)	(1.6)	(1.8)	(4.6)
$[N_2]$, mmol/l[c]	0.047	0.079	0.015	0.092	0.075
$[NO_3^-]/[NH_4^+]$[c]	3.4	4.6	1.2	0.9	1.7
% yield CO_2[c]	88	70	90	91	71
% yield ΣN_i[c]	70	98	41	74	65

[a]Induction period ca. 5–6 h.
[b]Induction period ca. 2 h.
[c]After 30 h of irradiation of the pyrimidine or purine base/TiO_2 dispersion.

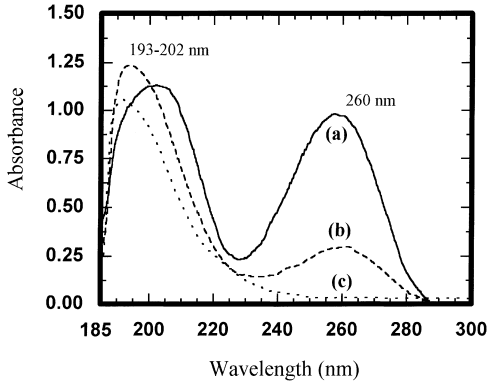

Fig. 2. Temporal changes in the UV absorption spectrum during the decomposition of uracil (0.1 mM): (a) 0 h, (b) 0.5 h, and (c) 1 h of irradiation.

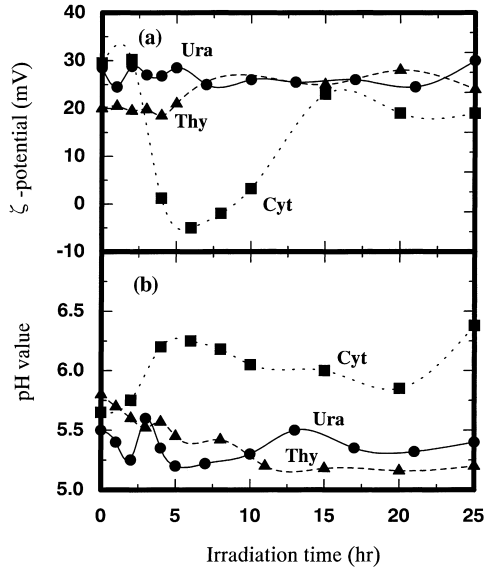

Fig. 3. (a) Graph illustrating the changes in ξ-potentials as a function of irradiation time for uracil, thymine, and cytosine; (b) pH changes during the photomineralization of uracil, thymine and cytosine.

attained during the first 8 h of irradiation. The intermediates of nitrogen-containing species photocleavaged would be present because of no stoichiometric decomposition for carbon moieties.

UV absorption spectral features of uracil at various irradiation times of the Ura/TiO_2 system are illustrated in Fig. 2. The band at 260 nm disappeared completely after 1 h of illumination. By comparison, the absorption band at 202 nm showed little if any variations in intensity, except for a slight blue-shift to $\sim$ 193 nm. Simulated calculations of the initial absorption spectrum of uracil by the ZINDO method gave the frontier electron densities and point charges for the nitrogen, carbon and oxygen atoms collected in Table 2. Results of the theoretical simulations suggest that the absorption feature at 260 nm in the experimental spectrum of Fig. 2 is largely due to UV absorption by the $O^7{=}C^1{-}C^2{=}C^3{-}N^6{-}$ fragment in the uracil structure; in particular, the ZINDO simulation revealed that the portion $-C^2{=}C^3{-}N^6-$ is the greater contributor to this band. By contrast, the $O^7{=}C^1{-}N^5-$, O^8, C^3 and $>C^4{=}O^8$ groups are the major contributors to the spectral feature in the 202–193 nm range.

The initial pH of the Ura/TiO_2 dispersion was 5.5 and during irradiation showed little changes staying around 5.4 ± 0.1 (Fig. 3(b)), i.e. below the pH at which the TiO_2 particles have a neutral surface charge (pI of TiO_2 used is $\sim$ 6.3). Protons formed in Eq. (2) maintain the surface of the TiO_2 particles positive. Accordingly, the atoms bearing the greater negative charge in the base are the preferential points of adsorption of the base to the positive surface of TiO_2, which should, therefore, facilitate attack of the base by the photogenerated surface-bound $^{\bullet}OH$ radicals. The zeta potential (ζ-potential) of the Ura/TiO_2 dispersion prior to irradiation was 28.5 mV, and on UV irradiation remained nearly constant at 27 ± 2 mV thereafter to 25 h of illumination (Fig. 3(a)). The small changes witnessed in the behavior of the ζ-potential paralleled changes in the primary amine (Fig. 1(a)), which might be expected for reaction(s) between $^{\bullet}OH$ radicals and uracil.

The atoms having the most negative charge in uracil are the O^8 and O^7 atoms, permitting the uracil base to adsorb by simple coulombic forces onto the Ti^{IV} surface ions through the two carbonyl groups $>C^1{=}O^7$ and $>C^4{=}O^8$ in a chelate-like configuration. The uracil atoms with the highest frontier electron density, namely the $-C^2{=}C^3{-}N^6-$ group positioned furthest from the TiO_2 surface will be subject to $^{\bullet}OH$ radical attack.

The position(s) for attack of $^{\bullet}OH$ radicals is consistent with the experimental data for the UV spectral analysis (see above) of the 260-nm absorption feature which disappears rather quickly in ca. 1 h. The photodegradation of uracil at these short times is initiated with $^{\bullet}OH$ attack of the alkene $-C^2{=}C^3-$ carbons and to a lesser extent of the N^6 atom. Moreover, the attenuated changes in the 202–193 nm features strengthen the notion that $^{\bullet}OH$ radicals do not attack the remaining groups $O^7{=}C^1{-}N^5-$ and $>C^4{=}O^8$ of the uracil structure in any significant way. The greater photomineralization yield of CO_2 evolution relative to the total quantity of NO_3^- and NH_4^+ ions, and N_2 gas produced lends credence to this view.

At the level of sophistication of the MOPAC calculations, we cannot be more precise as to the dominant position for $^{\bullet}OH$ radical attack of the uracil ring, and for that matter also of the other pyrimidine and purine base ring structures. As well, the calculations are silent as to the point of bond cleavage and break-up of the structure. We can only speculate on the basis of experimental evolution of carbon dioxide and conversion of the nitrogens. In keeping with these considerations, we hypothesize that break-up of the uracil ring originates from cleavage of the $=C^3{-}N^6-$ bond converting N^6 to a primary amine function and then rapidly to NH_4^+ ions and N_2 gas (Fig. 1), and the $O^7{=}C^1{-}C^2{=}C^3-$ carbons are rapidly converted to CO_2 accounting for the

nearly 70% of CO_2 formed in the first 5 h of irradiation. The remaining $>C^4=O^8$ carbon yields CO_2 at a slower rate (Table 1). The N^5 nitrogen is consequently the likely candidate for NO_3^- ion formation being furthest removed from the initial events (see structure and pictorial representation of the electron densities on the uracil atoms displayed in Table 2).

4.2. Thymine

Formation of NH_4^+ ($k \approx 0.02\ h^{-1}$) and NO_3^- ($k = 0.08 \pm 0.03\ h^{-1}$) ions produced during the temporal photooxidative decomposition of Thymine together with the evolution and disappearance of a primary amine are depicted in Fig. 4(a). The quantities of NH_4^+ ions and NO_3^- ions produced after the 30-h illumination period were 0.013 mM and 0.062 mM, respectively.

However, evolution of these two ionic species necessitated a $\sim$5-h irradiation period (induction period) before being detected, a period at which maximal formation of the primary amine was attained. The subsequent decrease of the concentration of the primary amine after this period coincides with the evolution of nitrate and ammonium ions. Approximately 60% of the total nitrogen present in thymine was transformed to N_2 gas ($k = 0.16 \pm 0.02\ h^{-1}$) after 30 h of irradiation (Fig. 4(b)), with the total photomineralization yield based on the nitrogen converted being 98%, the highest in the photooxidation of all the bases examined. Evolution of CO_2 also followed first-order growth kinetics ($k = 0.28 \pm 0.03\ h^{-1}$) producing 0.35 mmol/l of the gas after 30 h of illumination; mineralization yield $\sim$70% a good fraction of which (about 60%) achieved in the first 6 h of illumination.

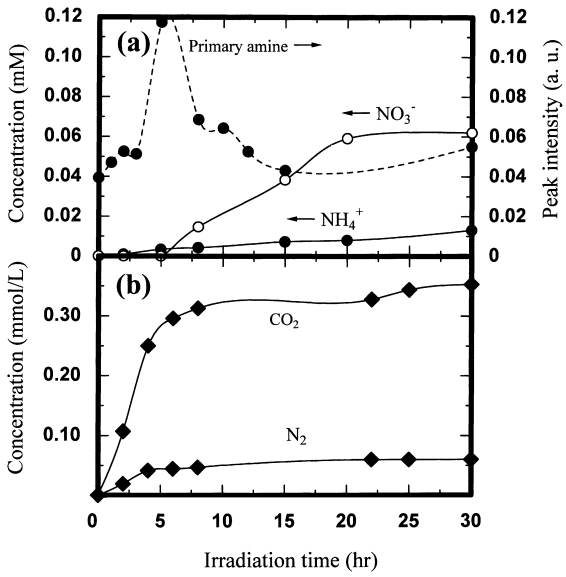

Fig. 4. Photodegradation of thymine (a): formation of NH_4^+ and NO_3^- ions, and generation of primary amine, (b): evolution of CO_2 and N_2 gas.

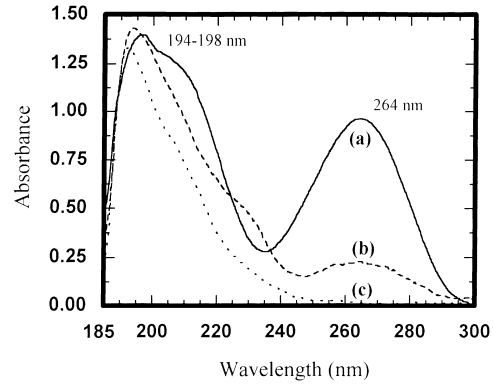

Fig. 5. Temporal changes in the UV absorption spectrum during the decomposition of thymine (0.1 mM): (a) 0 h, (b) 0.5 h, and (c) 1 h of irradiation.

The UV absorption spectrum of thymine displays two bands at 264 nm and in the 194–198 nm range. After 1 h of irradiation of the Thy/TiO_2 dispersion, only the spectral feature at 194–198 nm remained (Fig. 5). ZINDO simulation of the band at 264 nm shows that the electronic transition implicates states whose wave functions are formed mostly from the string of atoms $–C^2–C^3=C^4–N^7–$. By comparison, the spectral feature at 194–198 nm involves states whose principal contributors are the N^7 and C^3 atoms and the $O^8=C^5–N^6–C^2=O^1$ group; in particular the carbonyl oxygen atoms $O^1=C$ and $O^8=C$ bring the greatest contribution to the UV absorption below 200 nm.

The ζ-potential of the Thy/TiO_2 dispersion remained constant at 20 mV for the first 5 h of irradiation, following which it increased to $\sim$ 27.5 mV and by 25 h of irradiation the ζ-potential dropped to ca. 20 mV. The increase of the ζ-potential paralleled the change to more acidic pH's as also observed for the photodegradation of uracil. The maximum concentration of the primary amine was reached at the same irradiation time of ca. 5 h as for the increase of the ζ-potential and for the decrease of pH.

For a structure as similar as that of uracil, the pathway for the photooxidative mineralization of thymine (contains a $–CH_3$ group at the C^3 position; see Table 3) differs somewhat from that for Uracil with the total conversion of nitrogen atoms somewhat greater than conversion of the carbons to CO_2 gas (yields for CO_2 are 70 and 88%, respectively; for N conversion yields are 98 and $\sim$70%, respectively). During the first 8 h of illumination, the photomineralization to carbon dioxide was rather fast (see Fig. 4(b)). The atoms bearing the greatest negative charge in thymine are also the $–C^2=O^1$ and $–C^5=O^8$ oxygens; hence by analogy with uracil, thymine also adsorbs on the Ti^{IV} ions TiO_2 particle surface through the carbonyl oxygens in a chelating manner.

The position of attack by the $^{\bullet}OH$ radicals on the thymine structure can also be inferred from frontier electron densities, determined from the MOPAC calculations (Table 3), which show that the densities of the C^3, C^4 and N^7 atoms are greater than for all other atoms, with the N^7 nitrogen having

Table 2
Frontier electron densities and point charge calculations of uracil using the CAChe (MOPAC) system

Atom	Frontier electron density	Point charges
C1	0.20989	0.5080
C2	0.57848	−0.0630
C3	0.47347	0.1013
C4	0.10482	0.6360
N5	0.06900	−0.2782
N6	0.29618	−0.2918
O7	0.16365	−0.6452
O8	0.09687	−0.6578
H9	0.00047	0.0926
H10	0.00057	0.0958
H11	0.00342	0.2574
H12	0.00319	0.2449

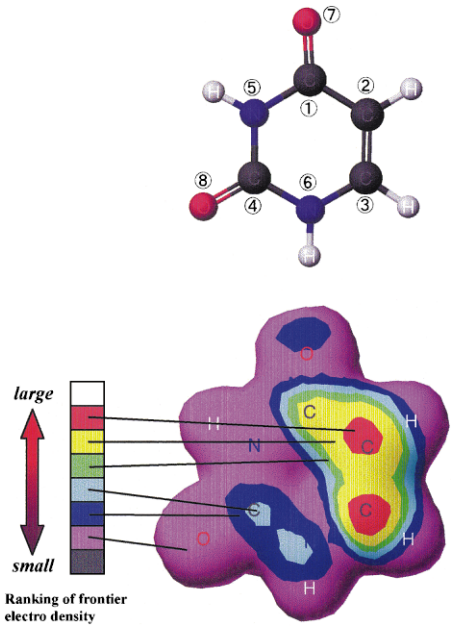

Table 3
Frontier electron densities and point charge calculations of thymine using the CAChe (MOPAC) system

Atom	Frontier electron density	Point charges
O1	0.13746	−0.6474
C2	0.19101	0.5051
C3	0.53874	0.0100
C4	0.49477	0.0754
C5	0.11434	0.6345
N6	0.06287	−0.2781
N7	0.25289	−0.2973
O8	0.08429	−0.6604
H9	0.04354	0.0615
H10	0.00056	0.0858
H11	0.00359	0.2560
H12	0.00315	0.2426
C13	0.03488	−0.0809
H14	0.03763	0.0619
H15	0.00028	0.0311

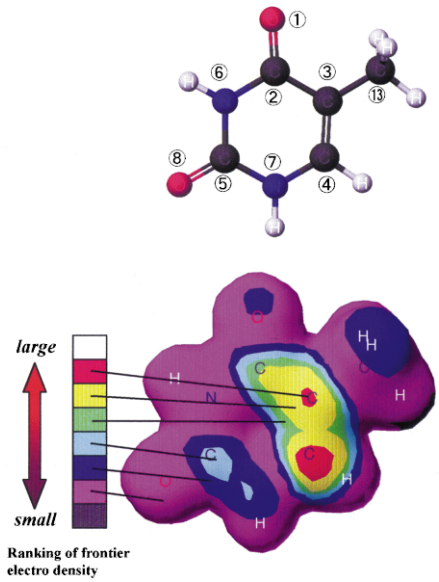

Table 4
Frontier electron densities and point charge calculations of cytosine using the CAChe (MOPAC) system

Atom	Frontier electron density	Point charges
C1	0.30369	0.3600
C2	0.45496	−0.0956
C3	0.37837	0.1212
C4	0.08039	0.6061
N5	0.12160	−0.4362
N6	0.26967	−0.4023
N7	0.30194	−0.2810
O8	0.08733	−0.6938
H9	0.00020	0.0585
H10	0.00035	0.0887
H11	0.00033	0.2094
H12	0.00036	0.2252
H13	0.00080	0.2398

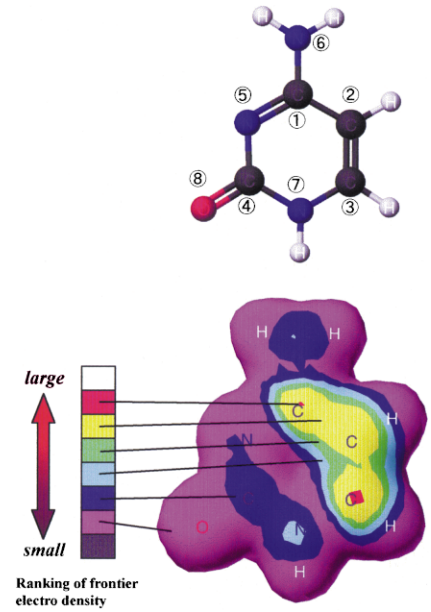

a significantly greater electron density (0.25289) than the N^6 nitrogen (0.06287). Consequently, the N^7 position of thymine might be a point of attack by $^{\bullet}OH$ radicals in a manner similar to the uracil base for the equivalent N^6 nitrogen (see Table 1). The frontier electron density for the C^4 carbon (0.49477) in thymine is greater than for the corresponding C^3 carbon (0.47342) in uracil, no doubt influenced by the presence of the C^{13} methyl group in the structure of thymine. The presence of this methyl group and the relative values of the electron densities suggest that propensity for $^{\bullet}OH$ radical attack on the thymine ring will likely be on the $>C^3=C^4–N^7$ group atoms. A more focused radical attack on the N^7 nitrogen than might occur on the uracil equivalent nitrogen N^6 is consistent with the greater conversion yields for N and formation of a greater quantity of NO_3^- ions for thymine than for uracil after the 30 h illumination period (0.062 mM versus 0.035 mM, respectively).

On the basis of the experimental observations then, we propose that the photooxidative transformation of thymine implicates three major processes: (i) adsorption of thymine on the TiO_2 particle surface through the two carbonyl oxygens, (ii) opening of the thymine ring structure by cleavage of the $=C^4–N^7–$ bond after attack by $^{\bullet}OH$ radicals on the $–C^3=C^4–N^7–$ positions as witnessed by the temporal changes taking place in the UV-spectral data (Fig. 5) during the first hour of illumination and in accord with the frontier electron densities of Table 3, and (iii) evolution of CO_2 and N_2 gases and formation of NH_4^+ and NO_3^- ions after an induction period of ca. 5 h.

4.3. Cytosine

The cytosine structure is distinct from that of uracil and thymine; it has a primary amine function on the C^1 carbon. Generation of NH_4^+ ($k = 0.6 \pm 0.2\ h^{-1}$) and NO_3^- ($k = 0.16 \pm 0.02\ h^{-1}$) ions along with the evolution of N_2 ($k \approx 0.4 \pm 0.2\ h^{-1}$) and CO_2 ($k = 0.32 \pm 0.03\ h^{-1}$) gases in the photocatalyzed degradation of cytosine are depicted in Fig. 6(a and b). Conversion of the nitrogens in the cytosine structure produced a greater quantity of NH_4^+ ions than NO_3^- ions for periods under 10–15 h of illumination (Fig. 6(a)), however, continued irradiation for up to 30 h led to nearly the same quantities of both ionic species: 0.015 mM of NH_4^+ ions and 0.018 mM of NO_3^- ions. The quantity of N_2 gas evolved was 0.045 mmol/l, which together with the nitrate and ammonium ions produced corresponds to a global mineralization yield of 41% (Table 1). By comparison, the quantity of CO_2 evolved was 0.36 mmol/l, giving a mineralization yield for the carbons of 90% after illumination for 30 h, more efficient than the equivalent transformation of the nitrogens. Moreover, CO_2 evolved promptly on irradiation (Fig. 6(b)) accounting for about 78% by ca. 8 h of illumination. The quantity of primary amine increased in the first 3 h and then decreased until it reached a constant concentration after about 10 h, at levels nearly identical with the initial concentration (Fig. 6(a)).

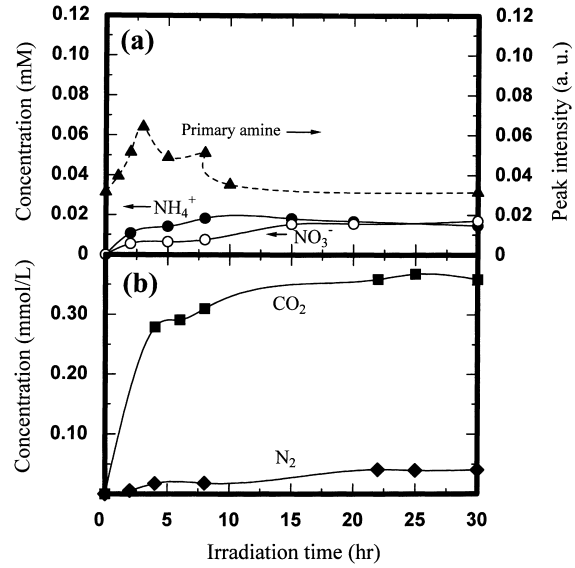

Fig. 6. Photodegradation of cytosine (a): formation of NH_4^+ and NO_3^- ions, and generation of primary amine, (b): evolution of CO_2 and N_2 gas.

The absorption spectrum of cytosine consists of two major UV bands, one in the range 196–198 nm and the other at 269 nm (Fig. 7), as well a shoulder at ca. 215 nm. Both bands decreased in intensity with increasing irradiation time with the 269-nm band completely disappearing after 1 h (the shoulder shifted to 230 nm after 0.5 h; spectrum b). The disappearance of the former UV band for cytosine finds no equivalence in the temporal behavior of the corresponding UV bands in uracil and thymine, both of which possess an otherwise identical ring skeleton to cytosine (see above). ZINDO simulation of the 269-nm band shows that the structural constituents that contribute to the states involved in this band are the O^8, C^3 and N^5 atoms, and the $–N^5=C^1<$ and $–C^2=C^3–N^7–$ groups. Similarly, the band at 198 nm also contains contributions from the O^8, C^1 and C^3 atoms, and from the C^2 and $O^8=C^4(–N^7)–N^5=$ functions. These results accord with the temporal decrease of the entire absorption

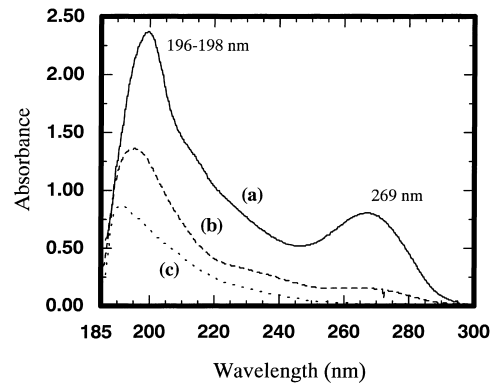

Fig. 7. Temporal changes in the UV absorption spectrum during the decomposition of cytosine (0.1 mM): (a) 0 h, (b) 0.5 h, and (c) 1 h of irradiation.

spectrum, unlike the uracil and thymine spectra where only the long wavelength band was affected (Figs. 2 and 5).

The initial pH of the Cyt/TiO_2 dispersion was 5.7, which on UV irradiation increased slightly and within 4 h reached a constant pH of 6.1 ± 0.2 (Fig. 3(b)) rendering the surface charge of the TiO_2 particles neutral (pI of TiO_2 used ~ 6.3). The ζ-potential of the initial cytosine solution containing TiO_2 particulates was 30 mV; it decreased to about -5 mV after 6 h of illumination, and on further UV exposure to 15 h and longer the potential increased to 20 ± 2 mV (Fig. 3(a)).

MOPAC calculations of the cytosine atoms indicate that the O^8 atom bears the largest negative point charge of any other atom in the structure (see Table 4). The frontier electron densities resulting from these calculations also predict the position(s) for attack of cytosine by $^{\bullet}OH$ radicals.

They implicate the atoms in the $\equiv C^1–C^2=C^3–N^7–$ group, particularly the C^2 atom which carries the largest frontier electron density (0.45496). Photomineralization of amino acids examined earlier [29] yielded predominantly NH_4^+ ions originating from the amino group. Cytosine adsorbs on the TiO_2 surface through non-coulombic interactions by the lone $C^4=O^8$ oxygen, followed by conversion of the amino group to NH_4^+ ions on the basis of UV-spectral data (Fig. 7) and frontier electron density results (Table 4). Subsequent steps involve opening of the ring by cleavage of the $C^3–N^7$ bond of the $–C^2=C^3–N^7–$ function (loss of the 269 nm band of Fig. 7), however, we cannot preclude, at least in part, cleavage of the $C^4–N^7$ bond from the $O^8=C^4(–N^7)–C^5$ group (198 nm band of Fig. 7) to generate additional primary amine in concert with NH_4^+ and NO_3^- ions and evolution of CO_2. Formation of N_2 required a 2 h induction period. Note that the point of ring opening need not be the expected primary position (i.e. the C^2 carbon) for $^{\bullet}OH$ radical attack of the base ring structure.

In the case of uracil and thymine, whose structures contain two carbonyl groups, formation of NO_3^- ions was detectable only after the primary amine had reached its maximal concentration. For cytosine, however, formation of NO_3^- ions required no induction period, i.e. it occurred during formation of additional primary amine(s), albeit the quantity of nitrate was rather small (Fig. 6(a)). Finally, by contrast with the other two pyrimidine bases for which at the conclusion of the 30-h illumination period the $[NO_3^-]/[NH_4^+]$ ratio is significantly greater than unity, for cytosine this ratio is close to unity (Table 1), no doubt influenced by the presence of the $–NH_2$ group which attenuates the formation of nitrate relative to ammonium ions.

5. Photodegradation of purine bases

Purine bases are structurally distinct from the pyrimidine bases consisting of a six-membered heteroring fused with a five-membered heteroring. Adenine and guanine both possess an amine function, contrary to uric acid (see above) which has a similar structural skeleton but with three carbonyl functions. Uric acid was examined to aid in the delineation of the effects of the amine group and the carbonyls with regard to conversion of the nitrogens in the three structures.

5.1. Adenine

Formation of NH_4^+ (0.10 mM; $k = 0.35 \pm 0.04\ h^{-1}$) and NO_3^- ions (0.088 mM; $k = 0.061 \pm 0.008\ h^{-1}$) and changes in the concentration of the primary amine for a 30-h illumination period are depicted in Fig. 8(a). Of all the bases examined, only for adenine was formation of NH_4^+ ions more significant than generation of NO_3^- ions. Formation of the latter displayed an induction period of ca. 2 h before detection. The amino group in adenine is predominantly converted to NH_4^+ ions by analogy with cytosine. Development of the primary amine exhibits two maximum peaks at 1 and 8 h of irradiation; continued illumination for 12 h and more leads to increased generation of the primary amine. Production of NO_3^- ions occurred concomitant with the loss of the primary amine produced in the first 2 h of irradiation, inferring a common nitrogen atom, initially at least in part.

The temporal evolution of N_2 and CO_2 in the photooxidation of adenine is illustrated in Fig. 8(b). The respective mineralization yields relative to N_2 ($k = 0.38 \pm 0.05\ h^{-1}$) and CO_2 ($k = 0.19 \pm 0.03\ h^{-1}$) are 37 and 91%, respectively, with the quantity of CO_2 evolved (0.45 mmol/l) being the highest observed for all the bases surveyed. The total photoconversion yield (NH_4^+, NO_3^- and N_2) of the nitrogen atoms in adenine is 74% at the conclusion of the 30-h irradiation period.

The UV absorption spectrum of adenine (Fig. 9) exhibits two bands one at 207 nm and other at 260 nm. ZINDO

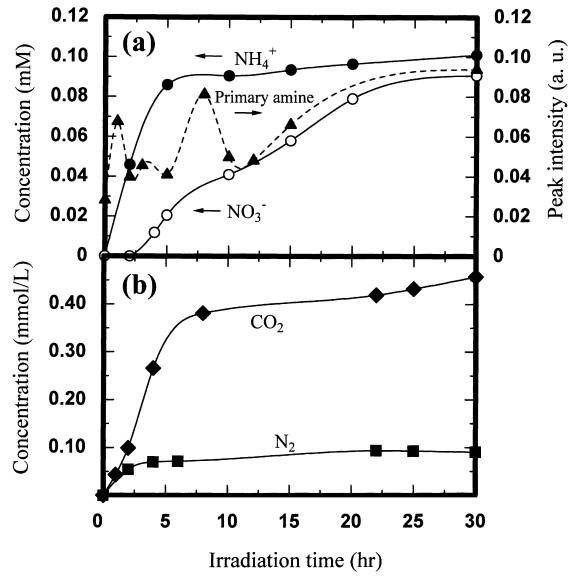

Fig. 8. Photodegradation of adenine (a): formation of NH_4^+ and NO_3^- ions, and generation of primary amine, (b): evolution of CO_2 and N_2 gas.

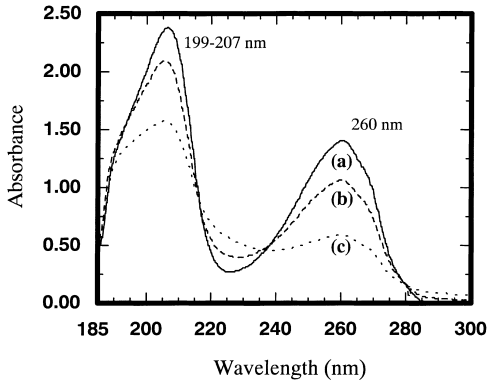

Fig. 9. Temporal changes in the UV absorption spectrum during the decomposition of adenine (0.1 mM): (a) 0 h, (b) 0.5 h, and (c) 1 h of irradiation.

simulation of these bands indicates that the groups $>C^1=N^9-$, C^5 and $=N^8-C^3-$ contribute the most to the band at 260 nm, whereas the 207 nm band contained mostly contributions from the $>C^1=N^9-$, C^5, N^6 and C^3 functions. After 1 h of exposure of the Ade/TiO_2 dispersion to UV radiation, there remains a significant residual absorption at 260 nm and 207 nm, unlike the pyrimidine bases where the former equivalent bands completely disappeared (see above). Evidently, contribute OH radical attack at these adenine functions must be attenuated somewhat.

The pH of the dispersion changed from ~ 5.8 to 6.3 ± 0.1 immediately on UV-irradiation shifting the surface charge of TiO_2 from positive to a neutral condition (note the point of zero charge, pI, of TiO_2 occurs at pH ≈ 6.3); see Fig. 10(b). The ξ-potential for the solution of adenine containing TiO_2 initially registered as ~ 6.5 mV decreasing in the first 6 h of UV irradiation to -2 mV. On further exposure to UV radiation, the ξ-potential increased back to 21 mV after 10 h and decreasing to 14 mV after 25 h (Fig. 10(a)).

Results of point charge and frontier electron density calculations (Table 5) of the atoms in adenine show that the N^6, N^8, N^9 and N^{10} atoms bear the largest negative charge (-0.4074 to -0.4433). By comparison, the atoms bearing the largest electron densities and thus most prone to attack by $^{\bullet}OH$ radicals are the C^2, C^3, C^4 and C^5 carbons; the nitrogens N^8 and N^{10} also have significant electron densities, otherwise similar to the carbons. We infer that adsorption of adenine to TiO_2 probably takes place through the N^6 and N^{10} nitrogens by non-coulombic forces.

The principal source of NH_4^+ ions is the amino group at N^{10}, by analogy with amino acids [29]. Competitive contribute OH attack at the $>C^2=C^3<$ carbons and at the $>C^4=N^8-$ function will ultimately lead to opening of the two rings and to mineralization of the carbons to CO_2 and the nitrogens to N_2, NH_4^+ and NO_3^- species.

5.2. Guanine

Fig. 11(a) illustrates the temporal generation of NH_4^+ ($k = 0.16 \pm 0.02\ h^{-1}$) and NO_3^- ($k = 0.018 \pm 0.006\ h^{-1}$)

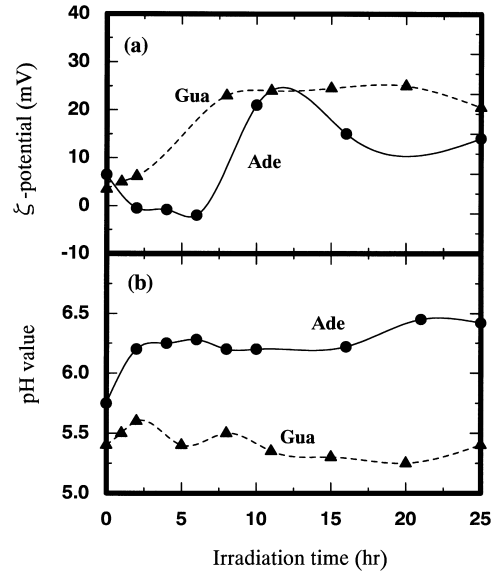

Fig. 10. (a) Graph illustrating the changes in ξ-potentials as a function of irradiation time for adenine and guanine; (b) pH changes during the photomineralization of adenine and guanine.

ions and the otherwise small increasing trend in the concentration of the primary amine during the photooxidative mineralization of guanine. Evolution of carbon dioxide ($k = 0.23 \pm 0.04\ h^{-1}$) and nitrogen ($k = 0.15 \pm 0.04\ h^{-1}$) is depicted in Fig. 11(b). After 30 h of illumination, the NH_4^+ ion concentration reached 0.065 mM and 0.11 mM for NO_3^- ions. A fraction of the NH_4^+ ions produced descend from the amino group at N^{11} (see Table 6). The mineralization yields of N_2 and CO_2 are 30 and 71%, respectively. Evolution of CO_2 gas was nearly 82% complete by 6 h of illumination. Total conversion yield of all nitrogen atoms

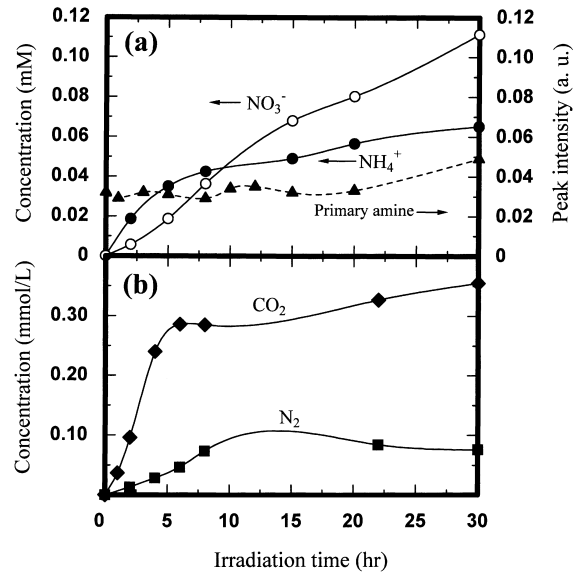

Fig. 11. Photodegradation of guanine (a): formation of NH_4^+ and NO_3^- ions, and generation of primary amine, (b): evolution of CO_2 and N_2 gas.

Table 5
Frontier electron densities and point charge calculations of adenine using the CAChe (MOPAC) system

Atom	Frontier electron density	Point charges
C1	0.26416	0.3419
C2	0.29446	0.0701
C3	0.18864	0.2691
C4	0.24643	0.2633
C5	0.23903	0.2003
N6	0.11275	−0.4074
N7	0.05447	−0.2909
N8	0.22298	−0.4324
N9	0.09999	−0.4433
N10	0.27594	−0.4174
H11	0.00006	0.0819
H12	0.00011	0.1061
H13	0.00050	0.2338
H14	0.00020	0.2135
H15	0.00025	0.2115

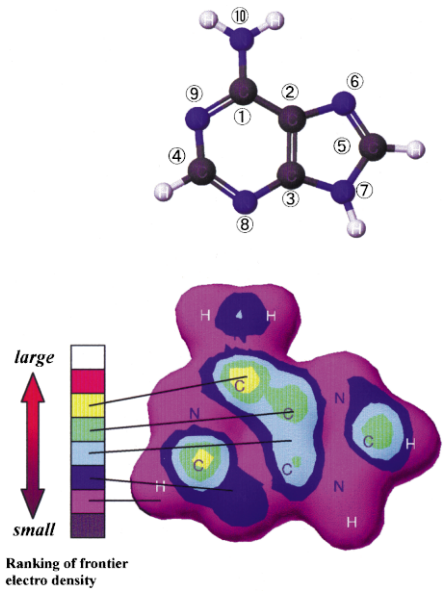

Table 6
Frontier electron densities and point charge calculations of guanine using the CAChe (MOPAC) system

Atom	Frontier electron density	Point charges
C1	0.1232	0.5063
C2	0.36135	0.0876
C3	0.28813	0.2462
C4	0.21511	0.1867
C5	0.31568	0.4492
N6	0.06987	−0.2858
N7	0.20053	−0.4510
N8	0.06944	−0.2869
N9	0.10684	−0.3642
O10	0.10213	−0.6771
N11	0.12838	−0.4033
H12	0.00001	0.1079
H13	0.00229	0.2344
H14	0.00033	0.2327
H15	0.00882	0.2046
H16	0.00785	0.2128

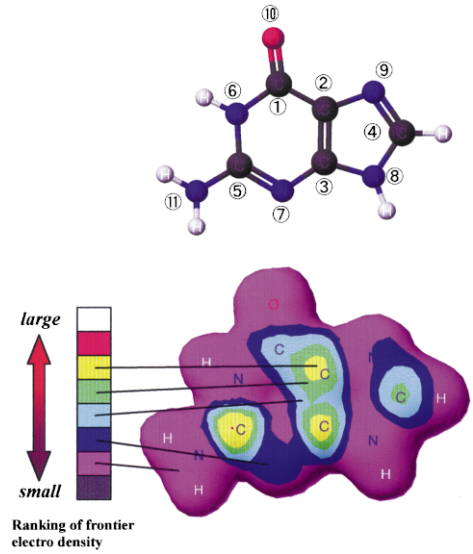

(NH_4^+, NO_3^- and N_2) reached 65% at the end of the 30-h irradiation period.

The three UV absorption bands observed in the spectrum of guanine at 199, 246 and 275 nm (Fig. 12) are different from those of other bases. The three bands decreased in intensity with irradiation time. The 275-nm band simulates with the $>C^1=O^{10}$ and C^5 functions, whereas the band at 246 nm is principally due to C^1 and the band at 199 nm arises mostly from contributions from the N^8, N^9, C^1, $\equiv C^5–N^6–$, C^2 and O^{10} atoms. Seemingly, the photodegradation of guanine concerns all ring atoms of guanine.

The pH of the Gua/TiO_2 aqueous dispersion was 5.4 ± 0.1 throughout the whole illumination period (Fig. 10(b)). Consequently the surface of TiO_2 remained positively charged. The initial ξ-potential of the Gua/TiO_2 aqueous dispersion was 3.5 mV; after 8 h of irradiation, it increased and remained constant at 23 ± 2 mV (Fig. 10(a)).

MOPAC calculations of point charges and frontier electron densities of the atoms in guanine are summarized in Table 6. The atoms with the largest negative charge in guanine are the N^7, N^9, O^{10} and N^{11} whereas the atoms with the greatest electron densities are C^2, C^3, C^4, C^5 and N^7. Hence, attack by $^{\bullet}OH$ radicals is expected to take place preferentially at these atoms.

By analogy with adenine, adsorption of guanine to TiO_2 occurs through the N^9 and O^{10} atoms occurring to some extent by coulombic forces. The subsequent step in the photodecomposition of guanine involves conversion of the amino group to NH_4^+ ions. Point charge and frontier electron density calculations suggest that the $>C^2=C^3<$ and/or $>C^5=N^7–$ bonds may be the most prone to $^{\bullet}OH$ radical attack and consequently a point of departure for the break-up of the guanine ring structure.

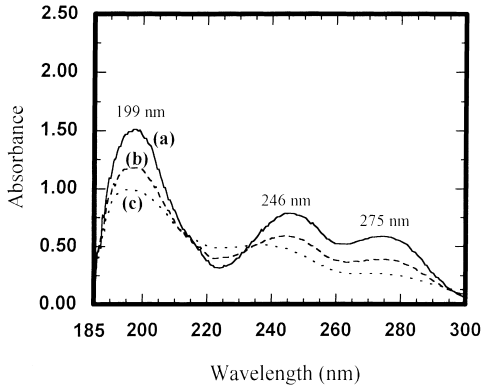

Fig. 12. Temporal changes in the UV absorption spectrum during the decomposition of guanine (0.1 mM): (a) 0 h, (b) 0.5 h, and (c) 1 h of irradiation.

5.3. Uric acid

Although uric acid has a skeletal structure similar to the purine bases, it lacks the amine group and has three carbonyl groups. Hence as a model system for purine bases, it can provide clues as the fate of the ring nitrogens under photocatalytic conditions. Most of the nitrogens are converted to NO_3^- ions (0.069 mM) and to a lesser extent to NH_4^+ ions (0.024 mM) by nearly a factor of 3 to 1 (Fig. 13(a)).

Comparing the evolution of NH_4^+ and NO_3^- ions in the photooxidation of uric acid to their evolution from the photomineralization of adenine and guanine, under otherwise identical experimental conditions (0.1 mM in a 50 ml dispersion), reveals that after 8 h the ratios $[NH_4^+]/[NO_3^-]$ for adenine, guanine and uric acid are, respectively, 2.2, 1.2 and 0.35. The larger ratios found for the purine bases indicate that a portion of the NH_4^+ ions originate definitely from the amino groups. The starting structure of uric acid has no primary amine, but the photodegradation of uric acid gave the formation of primary amine after 1 h and then the amount of primary amine kept constant.

The UV absorption spectrum of uric acid consists of a band at 231 nm and one at 285 nm (Fig. 13(b)). The latter band is also observed in the absorption spectra of alkenes. The shorter wavelength absorption feature decreases faster than the longer wavelength band; we assign this feature to $^{\bullet}OH$ attack predominantly on the carbonyl carbons and vicinal atoms. Frontier electron densities of the two carbons in the alkene bond are larger than those of other atoms (see e.g. Tables 2–6). The slower decrease of the 285-nm band must then be due to a less significant $^{\bullet}OH$ attack on the alkene carbons.

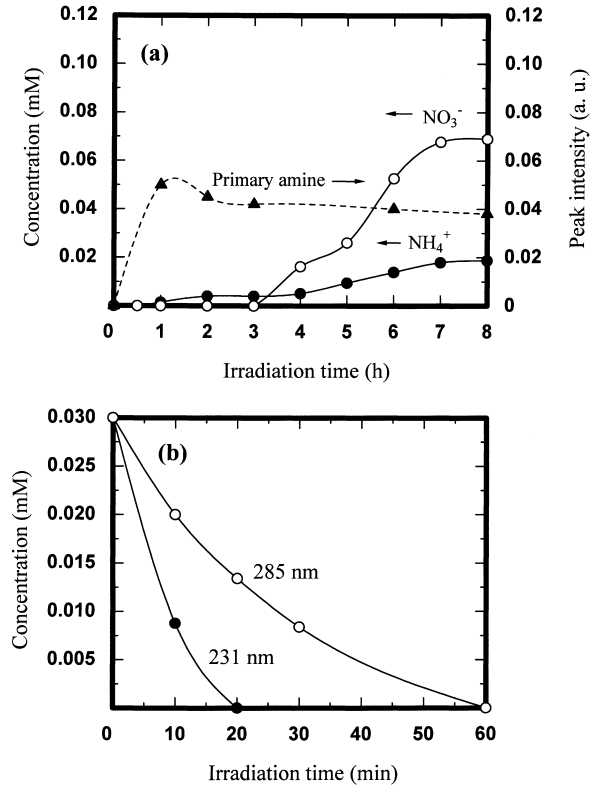

Fig. 13. (a) Formation of NH_4^+ ion, NO_3^- ions and temporal formation of primary amine in the photooxidation of uric acid (0.1 mM) in aqueous TiO_2 dispersion. (b) Disappearance of UV-absorption in the photodegradation of uric acid (initial concentration, 0.3 mM).

6. Conclusions

The photooxidative mineralization of the constituent pyrimidine and purine bases in nucleic acids together with MOPAC calculations of the point charges and frontier electron densities of all atoms in their respective structures have been examined. The three major mechanistic steps in the overall photooxidation of these bases are: (i) adsorption of the bases to the positively charge TiO_2 photocatalyst surface through the atoms bearing the greater negative charge; (ii) $^{\bullet}OH$ radical attack at ring atoms possessing the greater electron densities; and (iii) conversion of the carbons and nitrogens to carbon dioxide, and to ammonia, nitrate ions, and nitrogen, respectively. Those bases whose structures comprised initially also an amine function produced a greater quantity of NH_4^+ ions at least in the first few hours of irradiation. Ultimately, however, the proportion of NO_3^- ions to NH_4^+ ions becomes greater than unity. The principal source of nitrate ions originates from conversion, although not exclusively, of the ring nitrogen atoms. The photomineralization of carbon atoms in the bases was, in all cases, faster than conversion of the nitrogen atoms; evolution of N_2 must take place via a complicated sequence of intermediate processes which the present study has not identified.

Acknowledgements

This research was supported by Grants-in-aid for Scientific Research from the Ministry of Education (No. 10640569) and from the Environmental Protection Project

Foundation (to H.H.) and by the Natural Sciences and Engineering Research Council of Canada (to N.S.; No. A5443). This work was funded by the Sasakawa Scientific Research Grant from the Japan Science Society (to S.H.). The authors also thank T. Ohotuka and M. Mieda for their technical assistance.

References

[1] D.F. Ollis, H. Al-Ekabi, Photocatalytic Purification and Treatment of Water and Air, Elsevier, Amsterdam, 1993.
[2] H. Hidaka, H. Kubota, M. Gratzel, N. Serpone, Nouv. J. Chim. 9 (1985) 67.
[3] H. Hidaka, J. Zhao, E. Pelizzetti, N. Serpone, J. Phys. Chem. 96 (1992) 2226.
[4] J. Zhao, H. Hidaka, A. Takamura, E. Pelizzetti, N. Serpone, Langmuir 9 (1993) 1646.
[5] H. Hidaka, J. Zhao, Colloids and Surfaces 67 (1992) 165.
[6] H. Hidaka, K. Nohara, J. Zhao, N. Serpone, E. Pelizzetti, J. Photochem. Photobiol. A Chem. 64 (1992) 247.
[7] H. Hidaka, H. Jou, K. Nohara, J. Zhao, Chemosphere 25 (1992) 1589.
[8] E. Pelizzetti, M. Barbeni, E. Pramauro, N. Serpone, E. Borgarello, M.A. Jamieson, H. Hidaka, Chim. Ind. (Milan) 67 (1985) 623.
[9] H. Hidaka, Y. Suzuki, K. Nohara, S. Horikoshi, Y. Hisamatsu, E. Pelizzetti, N. Serpone, J. Polym. Sci., Part A, Polym. Chem. 34 (1996) 1311.
[10] S. Horikoshi, H. Hidaka, Y. Hisamatsu, N. Serpone, Environ. Sci. Technol. (1999) in press.
[11] S. Horikoshi, M. Ohta, H. Hidaka, J. Zhao, N. Serpone, Rec. Res. Dev. Polym. Sci., Transworld Res. Network, India 1 (1998) 149.
[12] S. Horikoshi, H. Hidaka, J. Jpn. Soc. Colour Mater. (SHIKIZAI) 71 (1998) 176.
[13] H. Hidaka, T. Nakamura, A. Ishizaka, M. Tsuchiya, J. Zhao, J. Photochem. Photobiol. A Chem. 66 (1992) 367.
[14] N. Serpone, Y.K. Ah-You, T.P. Tran, R. Harris, E. Pelizzetti, H. Hidaka, Sol. Energy 39 (1987) 491.
[15] D. Lawless, A. Res, R. Harris, N. Serpone, C. Minero, E. Pelizzetti, H. Hidaka, Chim. Ind. (Milan) 72 (1990) 139.
[16] T. Matsunaga, R. Tomoda, T. Nakajima, H. Wake, FEMS Microbiol. Lett. 29 (1985) 211.
[17] T. Matsunaga, R. Tomoda, T. Nakajima, N. Nakamura, T. Komine, Appl. Environ. Microbiol. 54 (1988) 1330.
[18] N. Laot, N. Narkis, I. Neeman, R. Armon, Third International Conference on TiO_2 Photocatalytic Purification and Treatment of Water and Air, Orlando, FL, September 1997.
[19] T. Matsunaga, M. Okochi, Environ. Sci. Technol. 29 (1995) 501.
[20] R.J. Watts, S. Kong, M.P. Orr, G.C. Miller, B.E. Henry, Water Res. 29 (1995) 95.
[21] T. Saito, T. Iwase, J. Horie, T. Orioka, J. Photochem. Photobiol. B Biol. 14 (1992) 369.
[22] P. Zhang, R.J. Scrudato, G. Germano, Chemosphere 28 (1994) 607.
[23] C. Wei, W.Y. Lin, Z. Zainal, N.E. Williams, K. Zhu, A.P. Kruzic, R.L. Smith, K. Rajeshwar, Environ. Sci. Technol. 28 (1994) 943.
[24] R. Cai, K. Hashimoto, K. Itoh, Y. Kubota, A. Fujishima, Bull. Chem. Soc. Jpn. 64 (1991) 1268.
[25] R. Cai, Y. Kubota, T. Shuin, H. Sakai, K. Hashimoto, A. Fujishima, Cancer Res. 52 (1992) 2346.
[26] R. Cai, K. Hashimoto, Y. Kubota, A. Fujishima, Chem. Lett. (1992) 427.
[27] H. Sakai, R. Baba, K. Hashimoto, Y. Kubota, A. Fujishima, Chem. Lett. (1995) 185.
[28] R. Dunford, A. Salinaro, L. Cai, N. Serpone, S. Horikoshi, H. Hidaka, J. Knowland, FEBS Lett. 418 (1997) 87.
[29] H. Hidaka, S. Horikoshi, K. Ajisaka, J. Zhao, N. Serpone, J. Photochem. Photobiol. A Chem. 108 (1997) 197.
[30] N. Serpone, A. Salinaro, S. Horikoshi, H. Hidaka, R. Dunford, J. Knowland, Proc. ASES Meeting (1998) in press.